MATERIALS SCIENCE

Superconducting praseodymium superhydrides

Di Zhou[1]*, Dmitrii V. Semenok[2]*, Defang Duan[1]*, Hui Xie[1], Wuhao Chen[1], Xiaoli Huang[1†], Xin Li[1], Bingbing Liu[1], Artem R. Oganov[2,3†], Tian Cui[4,1†]

Superhydrides have complex hydrogenic sublattices and are important prototypes for studying metallic hydrogen and high-temperature superconductors. Previous results for LaH_{10} suggest that the Pr-H system may be especially worth studying because of the magnetism and valence-band *f*-electrons in the element Pr. Here, we successfully synthesized praseodymium superhydrides (PrH_9) in laser-heated diamond anvil cells. Synchrotron x-ray diffraction analysis demonstrated the presence of previously predicted $F\bar{4}3m$-PrH_9 and unexpected $P6_3/mmc$-PrH_9 phases. Experimental studies of electrical resistance in the PrH_9 sample showed the emergence of a possible superconducting transition (T_c) below 9 K and T_c dependent on the applied magnetic field. Theoretical calculations indicate that magnetic order and likely superconductivity coexist in a narrow range of pressures in the PrH_9 sample, which may contribute to its low superconducting temperature. Our results highlight the intimate connections between hydrogenic sublattices, density of states, magnetism, and superconductivity in Pr-based superhydrides.

INTRODUCTION

The idea that hydrogen-rich compounds may be high–critical temperature (T_c) superconductors can be traced back to 2004 (*1*), when chemical precompression of hydrogen by other elements was proposed as an effective way to reduce the metallization pressure of hydrogen. Recent experimental results of T_c exceeding 200 K in compressed H_3S (*2*–*4*) and 250 to 260 K in LaH_{10} system (*5*–*8*) have indicated compressed hydrogen-rich compounds as potential room-temperature superconductors.

It is recognized that superconductivity in these hydrides owes its origin to electron-phonon coupling (EPC). Three parameters determine T_c: the characteristic phonon frequency, EPC, and Coulomb pseudopotential (*9*). Recent theoretical studies have covered almost all binary hydrides and found several metal superhydrides with extraordinary high-T_c superconductivity, such as CaH_6 (*10*), MgH_6 (*11*), YH_{6-10} (*12*, *13*), AcH_{10-16} (*14*), and ThH_{9-10} (*15*). Peng *et al.* (*16*) first studied all the candidate structures of rare earth superhydrides with H-rich cages at high pressure and proposed that only several hydrides could be superconductors with $T_c > 77$ K. At the same time, superhydrides with H_2 units are recognized to have relatively low critical temperature, e.g., LiH_6 (*17*), NaH_7 (*18*), $Xe(H_2)_7$ (*19*), and $HI(H_2)_{13}$ (*20*). The question is why some superhydrides are high-T_c superconductors, while others, with the same structure and stoichiometry, are not.

Continuing studies of lanthanide superhydrides, in this work, we studied high-pressure behavior of the Pr-H system above 100 GPa. Chesnut and Vohra (*21*) studied the crystal structure of metallic Pr and determined the phase sequence above megabar pressure. Pr can readily absorb hydrogen at high temperature and form hydrides: Face-centered cubic dihydride PrH_2 and hexagonal close-packed trihydride PrH_3 were found at ambient pressure. Subsequent filling of octahedral voids in the structure of dihydrides leads to nonstoichiometric PrH_{2+x} composition, which exhibits considerable variations of magnetic structures (*22*). Here, through high-pressure and high-temperature (HPHT) synthesis, two unexpected Pr superhydrides were obtained and studied. In particular, we investigated superconducting behavior of synthesized Pr superhydrides by electrical resistance measurements. Theoretical calculations are used to unravel the relationship among their magnetic properties, electronic band structures, phonon spectra, and superconductivity. Comparison with already detailed studies of La and Ce superhydrides allows us to elucidate the great influence of metal atoms on superconductivity of superhydrides.

[1]State Key Laboratory of Superhard Materials, College of Physics, Jilin University, Changchun 130012, China. [2]Skolkovo Institute of Science and Technology, Skolkovo Innovation Center 143026, 3 Nobel Street, Moscow, Russia. [3]International Center for Materials Discovery, Northwestern Polytechnical University, Xi'an 710072, China. [4]School of Physical Science and Technology, Ningbo University, Ningbo 315211, China.
*These authors contributed equally to this work.
†Corresponding author. Email: huangxiaoli@jlu.edu.cn (X.H.); a.oganov@skoltech.ru (A.R.O.); cuitian@jlu.edu.cn (T.C.)

RESULTS AND DISCUSSION

The stability and structures predicted by theoretical calculations

Before describing the experimental results, we have compared our theoretical findings with the previous ab initio study (*16*), which is different from ours in a number of aspects. These differences are crucial for understanding our experimental results and motivated us to further perform independent variable-composition searches for stable compounds in the Pr-H system at pressures of 50, 100, and 150 GPa using the Universal Structure Predictor: Evolutionary Xtallography (USPEX) (*23*–*25*) package and Ab Initio Random Structure Searching (AIRSS) (*26*) code (see fig. S1). The current theoretical results performed by Vienna Ab-initio Simulation Package (VASP) (*27*–*29*) are also checked by an independent code Cambridge serial total energy package (CASTEP) (*30*). The results of CASTEP can be found in fig. S1. These two codes give the same results in principle. The only difference is the symmetry of PrH_3 that CASTEP gives $C2/m$-PrH_3, while VASP gives $Pm\bar{3}m$-PrH_3 without magnetism and spin-orbit coupling (SOC) effects.

Results of the structure search exhibit large differences depending on including or excluding magnetism and SOC effects, which can be seen in Fig. 1 and fig. S1. However, previous calculations (*16*) did not include these effects. In agreement with previous results (*16*), our search gives $Pm\bar{3}m$ as the most stable symmetry for monohydride PrH and $Fm\bar{3}m$ for trihydride PrH_3, but important metastable phases $P4/nmm$-PrH_3 (~70 meV per atom above the convex hull) and $Fm\bar{3}m$-PrH were not reported. Previous work indicated that superhydride $F\bar{4}3m$-PrH_9 is stable between 100 and 200 GPa but did not report $P6_3/mmc$-PrH_9, which is about 19 meV per atom above the convex hull at 100 GPa. We also updated the convex hull and phase diagram of Pr-H system at 150 GPa.

Synthesis of polyhydrides $Fm\bar{3}m$-PrH_3 and $P4/nmm$-$PrH_{3-\delta}$

To synthesize previously unknown hydrides, we carried out several experiments by directly compressing Pr and hydrogen in the Diamond Anvil Cells (DACs). The diamond used in this experiment was coated with 150-nm alumina film by magnetron sputtering. The metallic Pr sample was loaded and sealed with a little pressure in the argon-protected glove box. After loading hydrogen into the cell, the sealed pressure was about 10 GPa, and selected x-ray diffraction (XRD) patterns are shown at various pressures (see fig. S3C). Figures 2 and 3 summarize the data for PrH_3 and PrH_9, respectively. Before laser heating, the diffraction pattern at 30 GPa included peaks from $Fm\bar{3}m$-PrH_3 in Fig. 2A, the structure of which can be viewed as cubic close packing of Pr atoms with all octahedral and tetrahedral voids filled by H atoms (see Fig. 2C). After compression to 40 GPa, the sample was laser-heated to 1400 K. We found stronger signal from $Fm\bar{3}m$-PrH_3, while peaks from $Fm\bar{3}m$-PrH disappeared (see fig. S3C). Upon further compression, the diamonds broke.

The experimental volumes of cubic PrH_3 are in good agreement with those predicted for $Fm\bar{3}m$-PrH_3 structure in the pressure range of 10 to 53 GPa (see Fig. 3B).The experimental equation of state (EoS) of this phase was fitted by the third-order Birch-Murnaghan EoS, which gave V_0 = 37.7 (3) Å^3, K_0 = 113 (2) GPa, and K_0' = 3.0 (5). $Fm\bar{3}m$-PrH, proposed for explanation of the XRD pattern, is slightly nonstoichiometic from the EoS (Fig. 3C), and it seems more correct to define as $Fm\bar{3}m$-PrH_{1+x}, where x = 0.08 to 0.13.

It is well known that experimental studies of hydrides are greatly affected by the hydrogen permeability contributing to the failure of diamonds in the high-pressure experiments. To minimize this problem, we synthesized the new hydrides by replacing of pure hydrogen with ammonia borane (AB), which is an excellent source of hydrogen (released during decomposition of AB). Several experiments were performed according to the reaction: $Pr + NH_3BH_3 \rightarrow PrH_x + c\text{-}BN$ through HPHT treatment (*31*–*33*). Figure 2B shows the diffraction pattern after laser heating at 43 GPa. The reaction products are dominated by $Fm\bar{3}m$-PrH_3 with a small quantity of tetragonal phase $P4/nmm$-$PrH_{3-\delta}$ ($0.05 \leq \delta \leq 0.15$) with smaller unit cell volume. At 50 GPa in the $P4/nmm$-PrH_3 structure, each Pr atom is bonded to 9 H atoms with 2.09 Å $\leq d$(Pr-H)$\leq$ 2.17 Å. Experimental cell parameters of found compounds are shown in table S3.

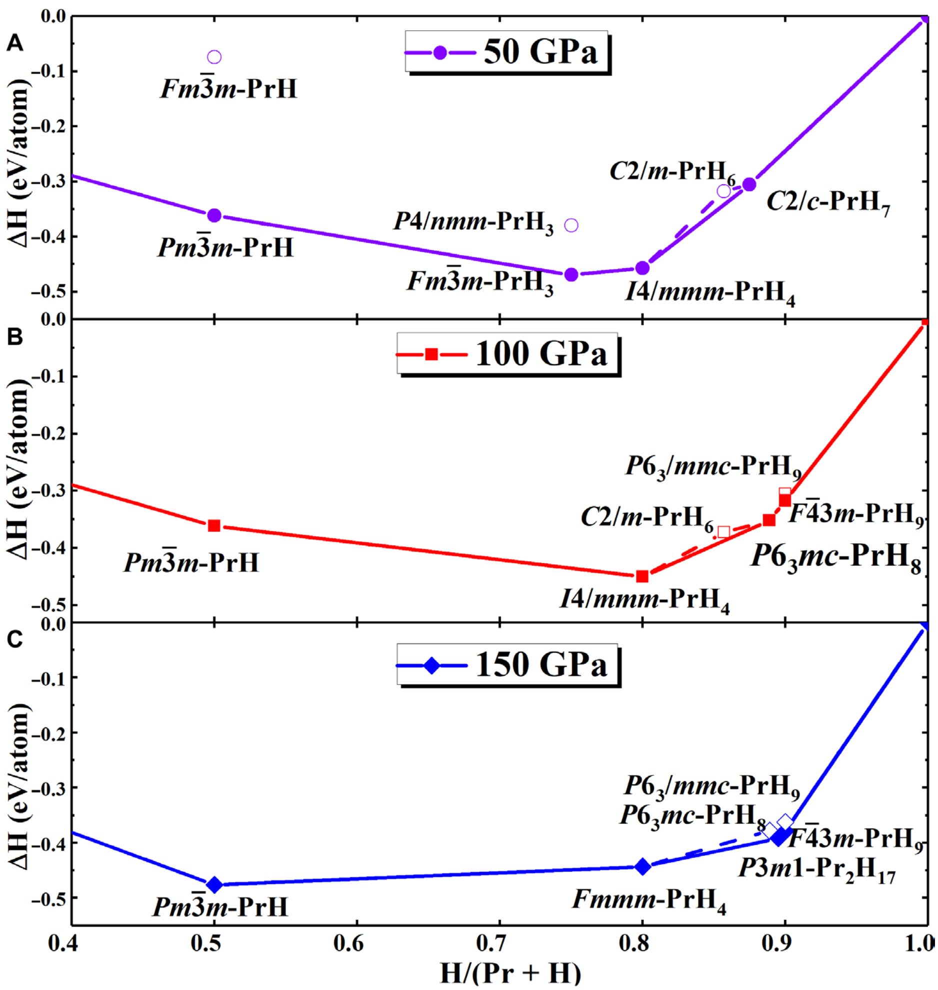

Fig. 1. Calculated convex hulls for Pr-H system at various pressures. Convex hulls for Pr-H system with the inclusion of SOC and magnetism at (**A**) 50, (**B**) 100, and (**C**) 150 GPa.

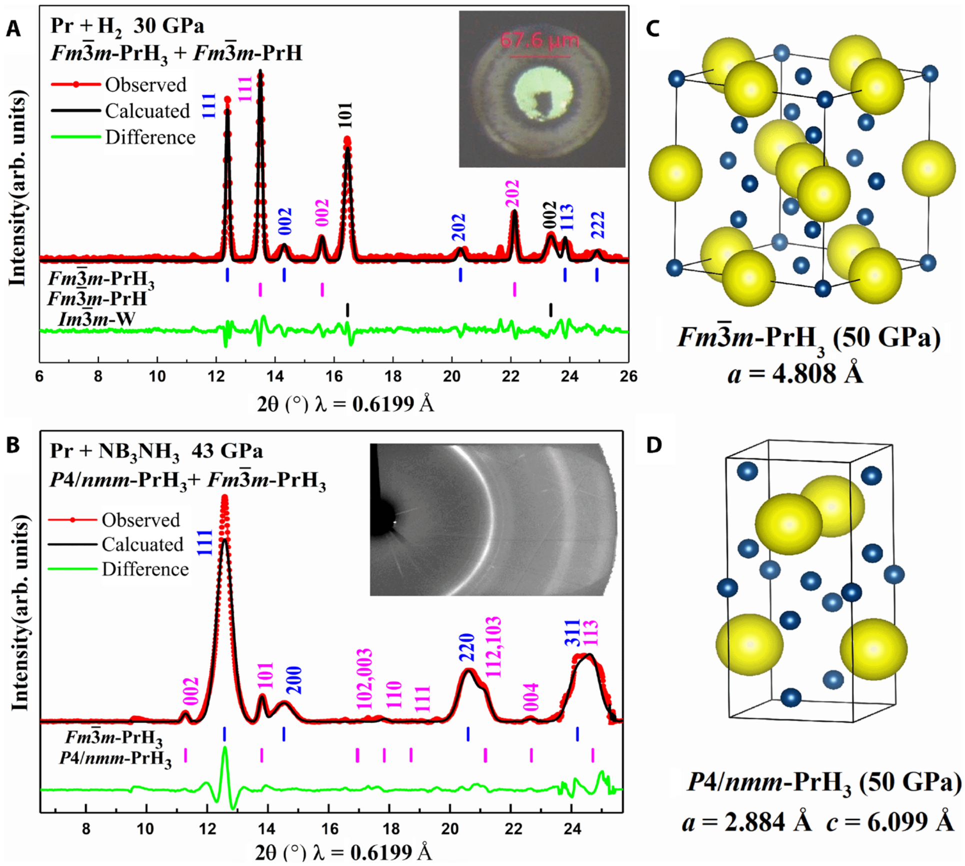

Fig. 2. XRD patterns and crystal structures of PrH_3 at pressures. (**A**) Refinement of the experimental XRD patterns obtained in Pr + H_2 cell by cold compression to 30 GPa. arb. units, means arbitrary units. (**B**) Refinement of the XRD pattern by *Fm*$\overline{3}$*m*-PrH_3 and *P4*/*nmm*-PrH_3 after laser heating at 43 GPa. Red line, experimental data; black line, model fit for the structure; green line, residues. R-factors for the refinement are $R_p = 14.2\%$ and $R_{wp} = 24.5\%$. Crystal structures of (**C**) *Fm*$\overline{3}$*m*-PrH_3 and (**D**) *P4*/*nmm*-PrH_3 phases at 50 GPa.

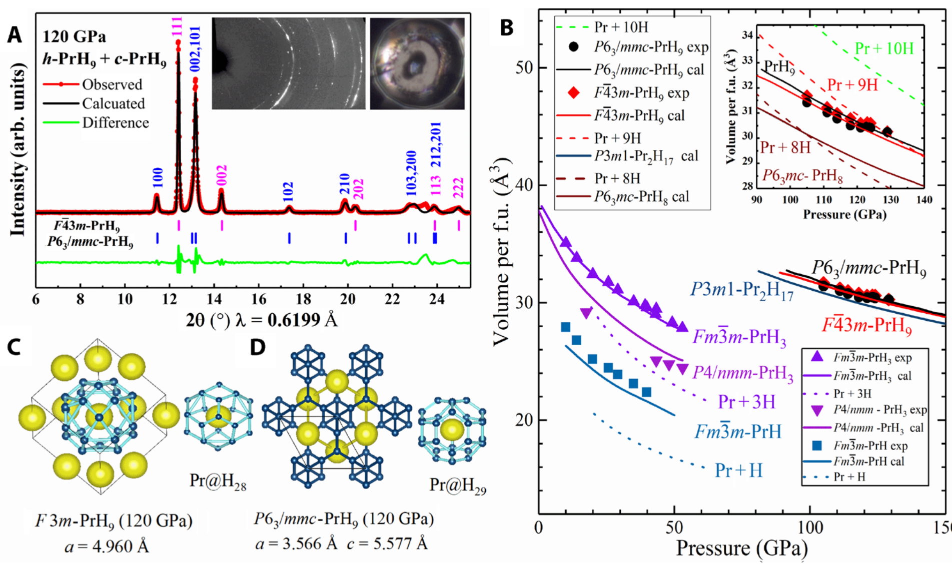

Fig. 3. Refinement of the experimental XRD pattern, pressure-volume data, and crystal structure of PrH_9. (**A**) Refinement of the XRD pattern by *F*$\overline{4}$3*m*-PrH_9 and *P*6_3/*mmc*-PrH_9. Red line, experimental data; black line, model fit for the structure; green line, residues. R-factors are as $R_p = 12.4\%$ and $R_{wp} = 22.0\%$. (**B**) EoS of the synthesized Pr-H phases; theoretical results include magnetism and SOC effects. Inset: The distinction among PrH_8, PrH_{10}, and PrH_9 phases. Crystal structures of (**C**) *F*$\overline{4}$3*m*-PrH_9 with H_{28} cages and (**D**) *P*6_3/*mmc*-PrH_9 with H_{29} cages.

Synthesis of $F\bar{4}3m$-PrH$_9$ and $P6_3/mmc$-PrH$_9$

To obtain higher hydrides of Pr, we conducted further experiments at pressures above 100 GPa. To overcome problems with hydrogen permeation, we also used NH_3BH_3 (AB) as the source of hydrogen, which proved to be effective for synthesis of superhydrides at megabar pressures (*7*, *34*). The original sample containing Pr with AB was laser-heated to 1650 K at 115 GPa. Measurements after laser heating did not show any changes in pressure, and Raman signal of H_2 was detected at 4147 cm^{-1}, indicating the generation of hydrogen. Figure 3A shows the XRD pattern with the presence of two praseodymium superhydrides $F\bar{4}3m$-PrH$_9$ and $P6_3/mmc$-PrH$_9$. Experimental lattice parameters at 120 GPa are a = 4.967 (1) Å and V = 122.52 (9) Å^3 for $F\bar{4}3m$-PrH$_9$ and a = 3.588 (1) Å, c = 5.458 (4) Å, and V = 60.84 (9) Å^3 for $P6_3/mmc$-PrH$_9$. This sample was compressed to 130 GPa and then gradually decompressed down to the lowest pressure of 105 GPa to determine its experimental EoS (Fig. 3B and table S4). Both EoS of PrH$_9$ are very close to the calculated curve of Pr + 9H and correspond well with the calculated values. After decompression down to 53 GPa, the recorded XRD pattern demonstrates the presence of two lower hydride phases: $Fm\bar{3}m$-PrH$_3$ with experimental parameters of a = 4.832 (1) Å at 50 GPa and $P4/nmm$-PrH$_{3\text{-}\delta}$ with a = 2.801 (1) Å and c = 6.280 (2) Å at 50 GPa, which is consistent with the low pressure results.

Both structures have almost the same volume and energy on convex hull at studied pressure range (Fig. 1, B and C). The stability of $F\bar{4}3m$-PrH$_9$ was previously predicted (*16*), while its coexistence with metastable $P6_3/mmc$-PrH$_9$ is unexpected. According to our theoretical calculations, the enthalpy difference between $P6_3/mmc$-PrH$_9$ and $F\bar{4}3m$-PrH$_9$ is about 19 meV per atom, which is near the limit of density functional theory (DFT) accuracy. According to recent studies (*35*, *36*), 20% of experimentally synthesized materials are metastable, some of which even have high positive formation enthalpy.

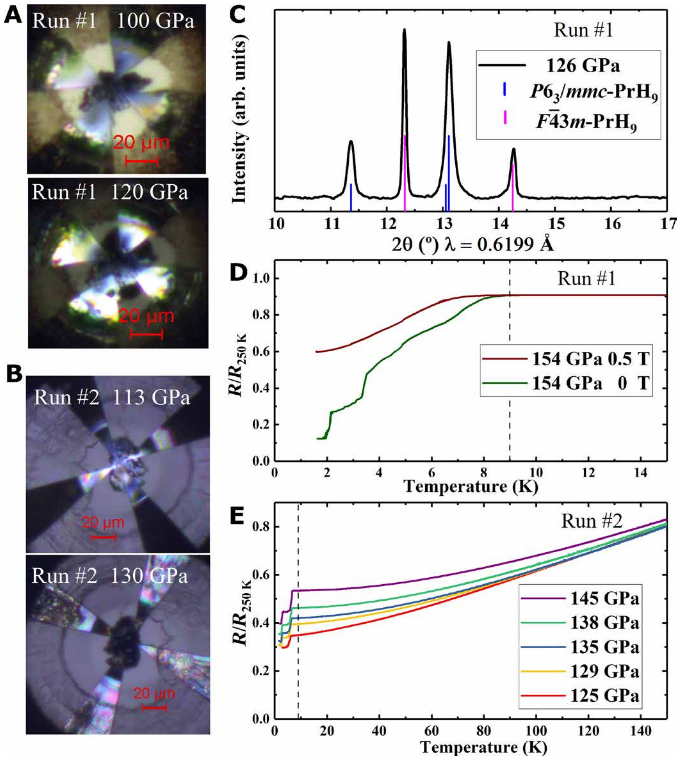

Fig. 4. Electrical resistance measurements of PrH$_9$. (**A**) The sample inside the diamond anvil cell connected with four electrodes before and after laser heating for sample 1. (**B**) The photos of sample 2 from different sides of cell after heating. (**C**) XRD pattern proves that cubic and hexagonal PrH$_9$ were synthesized in the sample at around 120 GPa from a mixture of Pr and AB. (**D**) Resistance steps of sample 1 at different magnetic fields. (**E**) Resistance steps of sample 2 at different pressures.

Properties of $F\bar{4}3m$-PrH$_9$ and $P6_3/mmc$-PrH$_9$

We performed a series of experiments to investigate superconductivity of PrH$_9$ via measurements of electrical resistance R(T) in the range of 1.6 to 300 K at pressures from 100 up to 150 GPa (see Fig. 4). The XRD pattern of the prepared sample at 126 GPa, deposited with four electrodes, shows presence of both $F\bar{4}3m$-PrH$_9$ and $P6_3/mmc$-PrH$_9$ phases (Fig. 4C). Possible superconducting transitions were detected with the resistance drop below 9 K, so we proposed that the superconducting transition temperature is below 9 K, far below LaH$_{10}$ of the same group. The superconducting resistance drop R(T) is also dependent on the applied magnetic field, further proving that this is a superconducting transition (see Fig. 4D). Another run of experiments confirmed the existence of the pronounced superconducting resistance drop in PrH$_9$ below 9 K (see Fig. 4E and fig. S9). The complexity of the experiments prevented us from accurately determining the pressure dependence of superconducting T_c. We did not observe zero resistance of the superhydrides samples due to their complex geometries, and the samples were mixed phase. The same phenomenon of incompletely dropping to zero in resistance have also been reported in the measurement of superconducting resistance of boron (*37*) and iron (*38*) at high pressure.

Further theoretical calculations were aimed at understanding why both $F\bar{4}3m$-PrH$_9$ and $P6_3/mmc$-PrH$_9$ have such low T_c. As shown in Fig. 3 (C and D), both structures have clathrate structures, which are also found in other rare earth hydrides. Calculations of the electron localization function reveal weak covalent H-H interactions. In $F\bar{4}3m$-PrH$_9$ structure, the nearest H-H distance is 1.135 Å at 120 GPa, which is a bit longer than the known shortest H-H distance in $P6_3/mmc$-CeH$_9$ (~1.1 Å) (*39*, *40*) but shorter than in $Fm\bar{3}m$-LaH$_{10}$ (*5*). At the same time, $P6_3/mmc$-PrH$_9$ with Pr@H$_{29}$ cages has the nearest H-H distance of ~1.170 Å (at 120 GPa), which is longer than d_{min}(H-H) in atomic hydrogen and in CeH$_9$ at the same pressure (for details, see fig. S4) (*16*).

Calculations demonstrate that both PrH$_9$ structures are dynamically stable (fig. S6) and exhibit metallic properties (Fig. 5). However, only 6 to 9% of the total densities of electron states (DOS) at the Fermi level comes from the hydrogen atoms, the rest being due to f-electrons of Pr. Relatively high values of the density of states above 3 to 4 eV^{-1} f.u.$^{-1}$ (per eV per formula unit) at or near (±1 eV) the Fermi level, caused by a series of Van Hove singularities make it impossible to use constant DOS approximation when calculating parameters of the superconducting state in PrH$_9$ (*41*). Low contribution of hydrogen to DOS is associated with weak EPC at 150 GPa, resulting in low superconducting T_c. EPC calculations for both PrH$_9$ with the selected pseudopotential (PP) give the estimated T_c of 0.8 K for cubic PrH$_9$ and 8.4 K for hexagonal PrH$_9$ at 120 GPa with μ* = 0.1, which is in good agreement with experiments (see figs. S10 to S12).

We summarized magnetic properties for all studied praseodymium hydrides at the pressure range of 0 to 150 GPa in Fig. 6. We find that all Pr-H compounds are magnetic: $Fm\bar{3}m$-PrH$_3$ and $Fm\bar{3}m$-PrH have strong magnetism and retain almost constant magnetic moments at high pressures, while tetragonal PrH$_3$ and both phases of PrH$_9$ lose magnetism under pressure. $P6_3/mmc$-PrH$_9$ loses magnetism at 120 GPa,

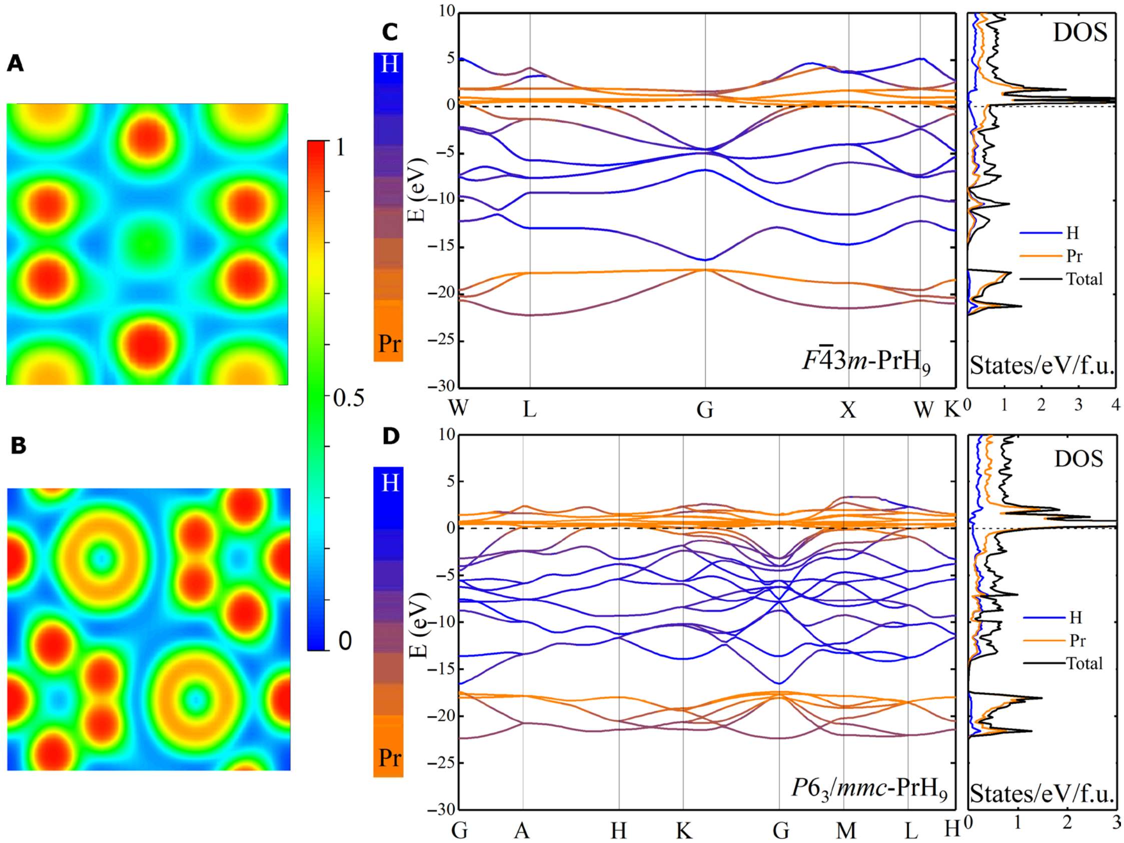

Fig. 5. Electronic properties of PrH_9. Electron localization function of (**A**) $F\bar{4}3m$-PrH_9 and (**B**) $P6_3/mmc$-PrH_9. Calculated DOS and band structure in (**C**) $F\bar{4}3m$-PrH_9 and (**D**) $P6_3/mmc$-PrH_9 at 150 GPa. DOS (E_F) is mostly due to *f*-electrons of Pr and has very high value in both cases.

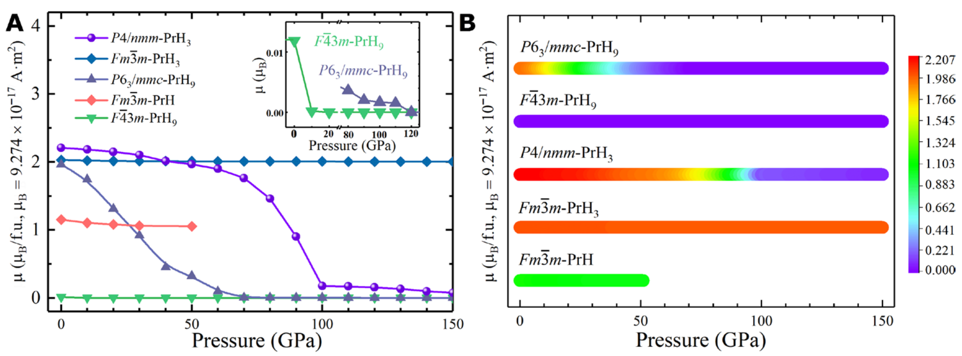

Fig. 6. Magnetism of Pr hydrides at pressures up to 150 GPa. (**A**) Magnetic moments of Pr-H compounds at high pressure and (**B**) magnetic map of Pr-H system as a function of pressure.

while $F\bar{4}3m$-PrH_9 retains a very low magnetic moment. Magnetic order and likely superconductivity coexist in a very close range of pressures in praseodymium hydrides, which may have an effect on the low superconducting transition temperature T_c.

CONCLUSIONS

Using in situ decomposition reaction of NH_3BH_3 under HPHT conditions previously used for synthesis of lanthanum superhydrides, we synthesized two novel metallic superhydrides $F\bar{4}3m$-PrH_9 and $P6_3/mmc$-PrH_9, two trihydrides $Fm\bar{3}m$-PrH_3 and $P4/nmm$-$PrH_{3\text{-}\delta}$, and one monohydride $Fm\bar{3}m$-PrH_{1+x} in the pressure range of 0 to 130 GPa. For most synthesized phases, the EoS and unit cell parameters are in good agreement with our DFT calculations. Resistance measurements of praseodymium hydrides indicated possible superconducting transitions in both PrH_9 below 9 K, which is in agreement with theoretical calculations: 8.4 K for hexagonal and 0.8 K for cubic PrH_9 at 120 GPa. Magnetic order and likely superconductivity coexist in a very close range of pressures in praseodymium hydrides, which may have an effect on the low superconducting transition temperature. Present results on Pr superhydrides show that superconductivity declines along the La-Ce-Pr series, while magnetism becomes more and more pronounced. Metallic atoms are not just donors of the electrons to the "metallic hydrogen" sublattice but play a more profound role in determining superconducting T_c.

METHODS

Experimental method

The praseodymium powder samples were purchased from Alfa Aesar with a purity of 99.99%. Molybdenum electrodes were sputtered onto the surface of one diamond anvils in the van der Pauw four-probe geometry. A four-probe measurement scheme was essential to separate the sample signal from the parasitic resistance of the current leads. We prepared an isolated layer from cubic boron nitride (or a mixture of epoxy and CaF_2). We performed laser heating of three diamond anvil cells (100- and 150-μm culets) loaded with metallic Pr sample and ammonia borane in the argon-protected glove box. The diamonds used for electrical DACs had a culet with a diameter of 100 μm. Thickness of the tungsten gasket was 20 ± 2 μm. Heating was carried out by pulses of infrared laser with a wavelength of 1 μm (Nd:YAG), and temperature measurements were carried out by the MAR 345 detector. Pressure was measured by the edge position of diamond Raman signal (*42*). XRD patterns studied in diamond anvil cells samples were recorded on the BL15U1 synchrotron beamline (*43*) at Shanghai Synchrotron Research Facility (China) with the use of a focused (5 μm × 12 μm) monochromatic beam. Additional syntheses with electrodes were carried out at the 4W2 High-Pressure Station of Beijing Synchrotron Radiation Facility (China). The beam size was about 32 μm × 12 μm. Both facilities are with the incident x-ray beam (20 keV, 0.6199 Å) and a Mar165 charge-coupled device two-dimensional detector. The experimental XRD images were integrated and analyzed using the Dioptas software package (*44*). The full profile analysis of the diffraction patterns, as well as the calculation of the unit cell parameters, was performed in the Materials Studio (*45*) and Jana2006 program (*46*) by the Le Bail method (*47*).

Theoretical calculations

We have carried out variable-composition searches for stable compounds in the Pr-H system at pressures of 50, 100, and 150 GPa using the USPEX (*23–25*) package coupled with the VASP code (*27–29*) and AIRSS (*26*) code coupled with the CASTEP plane-wave code (*30*) and on the fly pseudopotentials (*48*). The first generation of USPEX search (120 structures) was created using a random symmetric generator, while all subsequent generations (100 structures) contained 20% random structures and 80% created using heredity, soft mutation, and transmutation operators.

We calculated the EoS for PrH, both PrH_3, and two PrH_9 phases. To calculate the EoS, we performed structure relaxations of phases at various pressures using DFT (*49*, *50*) within the generalized gradient approximation (Perdew-Burke-Ernzerhof functional) (*51*, *52*) and the projector augmented-wave method (*53*, *54*) as implemented in the VASP code (*27–29*). Plane-wave kinetic energy cutoff was set to 1000 eV, and the Brillouin zone was sampled using Γ-centered k-points meshes with a resolution of $2\pi \times 0.05$ Å^{-1}. Obtained dependences of the unit cell volume on pressure were fitted by three-order Birch-Murnaghan equation (*55*) to determine the main parameters of the EoS, namely, V_0, K_0, and K', where V_0 is equilibrium volume, K_0 is bulk modulus, and K' is derivative of bulk modulus with respect to pressure using the EosFit7 software (*56*). We also calculated phonon densities of states for studied materials using finite displacement method [VASP (*57*) and Phonopy (*58*)].

Calculations of phonons, EPC, and superconducting T_c were carried out with Quantum ESPRESSO package (*59*) using density-functional perturbation theory (*60*), using plane-wave pseudopotential method and local density approximation exchange-correlation functional (*61*). Norm-conserving pseudopotentials for H ($1s^1$) and Pr ($5s^2 5p^6 4f^3 6s^2$) were used with a kinetic energy cutoff of 90 Rybderg (Ry). In our ab initio calculations of the EPC parameter λ, the first Brillouin zone was sampled using a 6 × 6 × 6 q-points mesh with a denser 24 × 24 × 24 k-points mesh for $F\bar{4}3m$-PrH_9 and a 3 × 3 × 2 q-points mesh with a denser 15 × 15 × 10 k-points mesh for $P6_3/mmc$-PrH_9 (with Gaussian smearing and σ = 0.035 Ry, which approximates the zero-width limits in the calculation of λ). Critical temperature T_c was calculated from the Allen-Dynes–modified McMillan formula (*62*) $T_c = \frac{\omega_{\log}}{1.2}\exp\left[-\frac{1.04(1+\lambda)}{\lambda-\mu^*(1+0.62\lambda)}\right]$, with $\omega_{\log} = \exp\left[\frac{2}{\lambda}\int \ln(\omega)\frac{\alpha^2F(\omega)}{\omega}d\omega\right]$ and $\lambda = 2\int\frac{\alpha^2F(\omega)}{\omega}d\omega$, where μ^*, $\alpha^2F(\omega)$, and λ are Coulomb pseudopotential, the electron-phonon spectral function, and the EPC parameter, respectively.

SUPPLEMENTARY MATERAILS

Supplementary material for this article is available at http://advances.sciencemag.org/cgi/content/full/6/9/eaax6849/DC1

Table S1. Crystal structure of predicted Pr-H phases.
Table S2. Experimental parameters of DACs.
Table S3. Experimental cell parameters and volumes of lower praseodymium hydrides along with calculated cell volumes (V_{DFT}).
Table S4. Experimental cell parameters and volumes of two praseodymium superhydrides along with calculated cell volumes (V_{DFT}).
Table S5. EoS of metallic Pr from reference.
Table S6. Calculated EoS parameters of third Birch-Murnaghan equation for all studied Pr-H phases.
Fig. S1. Calculated convex hulls for Pr-H system at various pressures.
Fig. S2. Convex hulls without and with zero-point energy (ZPE) correction of found praseodymium hydrides at 120 GPa.
Fig. S3. Experimental XRD patterns dependence of pressure in the range of 0 to 130 GPa.
Fig. S4. Pressure dependence of the nearest H-H distances and nearest Pr-H distances from experimental cell parameters.
Fig. S5. Raman spectra of Z1 cell under decompression.
Fig. S6. Calculated phonon density of states and band structure for PrH_9.
Fig. S7. Calculated phonon density of states and band structure for PrH_8 and PrH_3.
Fig. S8. Electron density of states for PrH_3.
Fig. S9. Enlarged figure of electrical resistance measurements of PrH_9 in sample 2.
Fig. S10. Calculated superconducting parameters of $F\bar{4}3m$-PrH_9 at 120 GPa as a function of electronic smearing σ and the pseudopotential.
Fig. S11. Eliashberg spectral functions, the electron-phonon integral λ(ω), and critical transition temperature $T_c(\omega)$ calculated at 120 GPa for cubic PrH_9 with σ = 0.035 Ry.
Fig. S12. Calculated superconductivity of hexagonal PrH_9 by Eliashberg spectral functions at 120 GPa.
References (*63–67*)

REFERENCES AND NOTES

1. N. W. Ashcroft, Hydrogen dominant metallic alloys: High temperature superconductors? *Phys. Rev. Lett.* **92**, 187002 (2004).
2. A. P. Drozdov, M. I. Eremets, I. A. Troyan, V. Ksenofontov, S. I. Shylin, Conventional superconductivity at 203 kelvin at high pressures in the sulfur hydride system. *Nature* **525**, 73–76 (2015).
3. M. Einaga, M. Sakata, T. Ishikawa, K. Shimizu, M. I. Erements, A. P. Drozdov, I. A. Troyan, N. Hirao, Y. Ohishi, Crystal structure of the superconducting phase of sulfur hydride. *Nat. Phys.* **12**, 835–838 (2016).
4. X. Huang, X. Wang, D. Duan, B. Sundqvist, X. Li, Y. Huang, H. Yu, F. Li, Q. Zhou, B. Liu, T. Cui, High-temperature superconductivity in sulfur hydride evidenced by alternating-current magnetic susceptibility. *Natl. Sci. Rev.* **6**, 713–718 (2019).
5. Z. M. Geballe, H. Liu, A. K. Mishra, M. Ahart, M. Somayazulu, Y. Meng, M. Baldini, R. J. Hemley, Synthesis and stability of lanthanum superhydrides. *Angew. Chem. Int. Ed.* **57**, 688–692 (2018).
6. M. Somayazulu, M. Ahart, A. K. Mishra, Z. M. Geballe, M. Baldini, Y. Meng, V. V. Struzhkin, R. J. Hemley, Evidence for superconductivity above 260 K in lanthanum superhydride. arXiv:1808.07695 [cond-mat.mtrl-sci] (23 August 2018).
7. M. Somayazulu, M. Ahart, A. K. Mishra, Z. M. Geballe, M. Baldini, Y. Meng, V. V. Struzhkin, R. J. Hemley, Evidence for superconductivity above 260 K in Lanthanum superhydride at Megabar pressures. *Phys. Rev. Lett.* **122**, 027001 (2019).
8. A. P. Drozdov, P. P. Kong, V. S. Minkov, S. P. Besedin, M. A. Kuzovnikov, S. Mozaffari, L. Balicas, F. F. Balakirev, D. E. Graf, V. B. Prakapenka, E. Greenberg, D. A. Knyazev, M. Tkacz, M. I. Eremets, Superconductivity at 250 K in lanthanum hydride under high pressures. *Nature* **569**, 528–531 (2019).

9. J. M. McMahon, D. M. Ceperley, High-temperature superconductivity in atomic metallic hydrogen. *Phys. Rev. B* **84**, 144515 (2011).
10. H. Wang, J. S. Tse, K. Tanaka, T. Iitaka, Y. Ma, Superconductive sodalite-like clathrate calcium hydride at high pressures. *Proc. Natl. Acad. Sci. U.S.A.* **109**, 6463–6466 (2012).
11. X. Feng, J. Zhang, G. Gao, H. Liu, H. Wang, Compressed sodalite-like MgH_6 as a potential high-temperature superconductor. *RSC Adv.* **5**, 59292–59296 (2015).
12. Y. Li, J. Hao, H. Liu, J. S. Tse, Y. Wang, Y. Ma, Pressure-stabilized superconductive yttrium hydrides. *Sci. Rep.* **5**, 9948 (2015).
13. H. Liu, I. I. Naumov, R. Hoffmann, N. W. Ashcroft, R. J. Hemley, Potential high-T_c superconducting lanthanum and yttrium hydrides at high pressure. *Proc. Natl. Acad. Sci. U.S.A.* **114**, 6990–6995 (2017).
14. D. V. Semenok, A. G. Kvashnin, I. A. Kruglov, A. R. Oganov, Actinium hydrides AcH_{10}, AcH_{12}, and AcH_{16} as high-temperature conventional superconductors. *J. Phys. Chem. Lett.* **9**, 1920–1926 (2018).
15. A. G. Kvashnin, D. V. Semenok, I. A. Kruglov, I. A. Wrona, A. R. Oganov, High-temperature superconductivity in a Th-H system under pressure conditions. *ACS Appl. Mater. Interfaces* **10**, 43809–43816 (2018).
16. F. Peng, Y. Sun, C. J. Pickard, R. J. Needs, Q. Wu, Y. Ma, Hydrogen clathrate structures in rare Earth hydrides at high pressures: Possible route to room-temperature superconductivity. *Phys. Rev. Lett.* **119**, 107001 (2017).
17. C. Pépin, P. Loubeyre, F. Occelli, P. Duma, Synthesis of lithium polyhydrides above 130 GPa at 300 K. *Proc. Natl. Acad. Sci. U.S.A.* **112**, 7673–7676 (2015).
18. V. V. Struzhkin, D. Y. Kim, E. Stavrou, T. Muramatsu, H. K. Mao, C. J. Pickard, R. J. Needs, V. B. Prakapenka, A. F. Goncharov, Synthesis of sodium polyhydrides at high pressures. *Nat. Commun.* **7**, 12267 (2016).
19. M. Somayazulu, P. Dera, A. F. Goncharov, S. A. Gramsch, P. Liermann, W. Yang, Z. Liu, H. K. Mao, R. J. Hemley, Pressure-induced bonding and compound formation in xenon–hydrogen solids. *Nat. Chem* **2**, 50–53 (2010).
20. J. Binns, P. Dalladay-Simpson, M. Wang, G. J. Ackland, E. Gregoryanz, R. T. Howie, Formation of H_2-rich iodine-hydrogen compounds at high pressure. *Phys. Rev. B* **97**, 024111 (2018).
21. G. N. Chesnut, Y. K. Vohra, Phase transformations and equation of state of praseodymium metal to 103 GPa. *Phys. Rev. B* **62**, 2965–2968 (2000).
22. P. Vajda, J. N. Daou, Rare Earths-hydrogen. *Solid State Phenom.* **49-50**, 71–158 (1996).
23. A. R. Oganov, C. W. Glass, Crystal structure prediction using ab initio evolutionary techniques: Principles and applications. *J. Chem. Phys.* **124**, 244704 (2006).
24. A. R. Oganov, R. O. Lyakhov, M. Valle, How evolutionary crystal structure prediction works-and why. *Acc. Chem. Res.* **44**, 227–237 (2011).
25. A. O. Lyakhov, A. R. Oganov, H. T. Stokes, Q. Zhu, New developments in evolutionary structure prediction algorithm USPEX. *Computer Phy. Commun.* **184**, 1172–1182 (2013).
26. C. J. Pickard, R. J. Needs, Ab initio random structure searching. *J. Phys. Condens. Matter* **23**, 053201 (2011).
27. G. Kresse, J. Hafner, Ab initio molecular dynamics for open-shell transition metals. *Phys. Rev. B* **48**, 13115–13118 (1993).
28. G. Kresse, J. Hafner, Ab initio molecular-dynamics simulation of the liquid-metal–amorphous-semiconductor transition in germanium. *Phys. Rev. B* **49**, 14251–14269 (1994).
29. G. Kresse, J. Furthmüller, Efficient iterative schemes for ab initio total-energy calculations using a plane-wave basis set. *Phys. Rev. B* **54**, 11169 (1996).
30. S. J. Clark, M. D. Segall, C. J. Pickard, P. J. Hasnip, M. I. J. Probert, K. Refson, M. C. Payne, First principles methods using CASTEP. *Z. Krist.-Cryst. Mater.* **220**, 567–570 (2005).
31. R. S. Chellappa, M. Somayazulu, V. V. Struzhkin, T. Autrey, R. J. Hemley, Pressure-induced complexation of NH_3BH_3–H_2. *J. Chem. Phys.* **131**, 224515 (2009).
32. Y. Song, New perspectives on potential hydrogen storage materials using high pressure. *Phys. Chem. Chem. Phys.* **15**, 14524–14547 (2013).
33. R. G. Potter, M. Somayazulu, G. Cody, R. J. Hemley, High pressure equilibria of dimethylamine borane, dihydridobis(dimethylamine)boron(III) tetrahydridoborate(III), and hydrogen. *J. Phys. Chem. C* **118**, 7280–7287 (2014).
34. D. V. Semenok, A. G. Kvashnin, A. G. Ivanova, V. Svitlyk, I. A. Troayn, A. R. Oganov, Superconductivity at 161 K in thorium hydride ThH_{10}: Synthesis and properties. *Mater. Today*, arXiv:1902.10206 [cond-mat.mtrl-sci] (26 February 2019).
35. Y. Wu, P. Lazic, G. Hautier, K. Perssonb, G. Ceder, First principles high throughput screening of oxynitrides for water-splitting photocatalysts. *Energ. Environ. Sci.* **6**, 157–168 (2013).
36. Y. Hinuma, T. Hatakeyama, Y. Kumagai, L. A. Burton, H. Sato, Y. Muraba, S. Iimura, H. Hiramatsu, I. Tanaka, H. Hosono, F. Oba, Discovery of Earth-abundant nitride semiconductors by computational screening and high-pressure synthesis. *Nat. Commun.* **7**, 11962 (2016).
37. M. I. Eremets, V. V. Struzhkin, H. Mao, R. J. Hemley, Superconductivity in boron. *Science* **293**, 272–274 (2001).
38. K. Shimizu, T. Kimura, S. Furomoto, K. Takeda, K. Kontani, Y. Onuki, K. Amaya, Superconductivity in the non-magnetic state of iron under pressure. *Nature* **412**, 316–318 (2001).
39. X. Li, X. Huang, D. Duan, C. J. Pickard, D. Zhou, H. Xie, Q. Zhuang, Y. Huang, Q. Zhou, B. Liu, T. Cui, Polyhydride CeH_9 with an atomic-like hydrogen clathrate structure. *Nat. Commun.* **10**, 3461 (2019).
40. N. P. Salke, M. M. D. Esfahani, Y. Zhang, I. A. Kruglov, J. Zhou, Y. Wang, E. Greenberg, V. B. Prakapenka, A. R. Oganov, J.-F. Lin, Synthesis of clathrate cerium superhydride CeH_9 at 80-100 GPa with anomalously short H-H distance. *Nat. Commun.* **10**, 4453 (2019).
41. W. Sano, T. Koretsune, T. Tadano, R. Akashi, R. Arita, Effect of Van Hove singularities on high-T_c superconductivity in H_3S. *Phys. Rev. B* **93**, 094525 (2016).
42. M. I. Eremets, Megabar high-pressure cells for Raman measurements. *J. Raman Spectrosc.* **34**, 515–518 (2003).
43. L.-L. Zhang, Y. Shuai, J. Sheng, Y. Ke, W. Hua, H. E. Shang-Ming, L. Dong-Xu, Z. Ling, H. E. Yan, L. Xu-Ying, M. Cheng-Wen, W. Juan, J. Hui, Z. Yi, D. Zhao-Hui, Z. Le-Yong, L. Ai-Guo, Hard x-ray micro-focusing beamline at SSRF. *Nucl. Sci. Tech.* **26**, 060101 (2015).
44. C. Prescher, V. B. Prakapenka, *DIOPTAS*: A program for reduction of two-dimensional x-ray diffraction data and data exploration. *High Pressure Res.* **35**, 223–230 (2015).
45. R. A. Young, The rietveld method. *Int. Union Cryst.* **30**, 494 (1995).
46. V. Petříček, M. Dušek, L. Palatinus, Crystallographic Computing System JANA2006: General features. *Z. Kristallogr.* **229**, 345–352 (2014).
47. A. L. Bail, H. Duroy, J. L. Forquet, Ab-initio structure determination of $LiSbWO_6$ by X-ray powder diffraction. *Mater. Res. Bull.* **23**, 447–452 (1988).
48. D. Vanderbilt, Soft self-consistent pseudopotentials in a generalized eigenvalue formalism. *Phys. Rev. B* **41**, 7892–7895 (1990).
49. P. Hohenberg, W. Kohn, Inhomogeneous Electron Gas. *Phys. Rev.* **136**, B864–B871 (1964).
50. W. Kohn, L. J. Sham, Self-consistent equations including exchange and correlation effects. *Phys. Rev.* **140**, A1133–A1138 (1965).
51. J. P. Perdew, K. Burke, M. Ernzerhof, Generalized gradient approximation made simple. *Phys. Rev. Lett.* **77**, 3865–3868 (1996).
52. J. P. Perdew, K. Burke, M. Ernzerhof, Generalized gradient approximation made simple [Phys. Rev. Lett. 77, 3865 (1996)]. *Phys. Rev. Lett.* **78**, 1396 (1997).
53. P. E. Blöchl, Projector augmented-wave method. *Phys. Rev. B* **50**, 17953–17979 (1994).
54. G. Kresse, D. Joubert, From ultrasoft pseudopotentials to the projector augmented-wave method. *Phys. Rev. B* **59**, 1758–1775 (1999).
55. F. Birch, Finite elastic strain of cubic crystals. *Phys. Rev.* **71**, 809–824 (1947).
56. J. Gonzalez-Platas, M. Alvaro, F. Nestola, R. Angel, EosFit7-GUI: A new graphical user interface for equation of state calculations, analyses and teaching. *J. Appl. Cryst.* **49**, 1377–1382 (2016).
57. A. Togo, F. Oba, I. Tanaka, First-principles calculations of the ferroelastic transition between rutile-type and$CaCl_2$-type SiO_2 at high pressures. *Phys. Rev. B* **78**, 134106 (2008).
58. A. Togo, I. Tanaka, First principles phonon calculations in materials science. *Scr. Mater.* **108**, 1–5 (2015).
59. P. Giannozzi, S. Baroni, N. Bonini, M. Calandra, R. Car, C. Cavazzoni, D. Ceresoli, G. L. Chiarotti, M. Cococcioni, I. Dabo, A. Dal Corso, S. de Gironcoli, S. Fabris, G. Fratesi, R. Gebauer, U. Gerstmann, C. Gougoussis, A. Kokalj, M. Lazzeri, L. Martin-Samos, N. Marzari, F. Mauri, R. Mazzarello, S. Paolini, A. Pasquarello, L. Paulatto, C. Sbraccia, S. Scandolo, G. Sclauzero, A. P. Seitsonen, A. Smogunov, P. Umari, R. M. Wentzcovitch, QUANTUM ESPRESSO: A modular and open-source software project for quantum simulations of materials. *J. Phys. Condens. Matter* **21**, 395502 (2009).
60. A. D. Becke, A new mixing of Hartree–Fock and local density-functional theories. *J. Chem. Phys.* **98**, 1372–1377 (1993).
61. J. P. Perdew, A. Zunger, Self-interaction correction to density-functional approximations for many-electron systems. *Phy. Rev. B* **23**, 5048–5079 (1981).
62. P. B. Allen, R. C. Dynes, Transition temperature of strong-coupled superconductors reanalyzed. *Phys. Rev. B* **12**, 905–922 (1975).
63. C. M. Pépin, G. Geneste, A. Dewaele, M. Mezouar, P. Loubeyre, Synthesis of FeH5: A layered structure with atomic hydrogen slabs. *Science* **357**, 382–385 (2017).
64. K. Conder, J. Schefer, E. Kaldis, C. Ru-Xiu, Progress in the T-X phase diagram of the solid solution CeH_2 — CeH_3. *Zeitschrift für Physik. Chem.* **163**, 125–134 (1989).
65. A. M. Rappe, K. M. Rabe, E. Kaxiras, J. D. Joannopoulos, Optimized pseudopotentials. *Phys. Rev. B* **41**, 1227–1230 (1990).
66. C. Heil, G. B. Bachelet, L. Boeri, Absence of superconductivity in iron polyhydrides at high pressures. *Phys. Rev. B* **97**, 214510 (2018).
67. C. Hartwigsen, S. Goedecker, J. Hutter, Relativistic separable dual-space Gaussian pseudopotentials from H to Rn. *Phys. Rev. B* **58**, 3641–3662 (1998).

Acknowledgments: We express gratitude to the staffs of BL15U and 4W2 stations of Shanghai and Beijing Synchrotron Radiation Facilities. **Funding:** This work was supported by the National Key R&D Program of China (grant no. 2018YFA0305900), National Natural Science Foundation of China (grant nos. 51632002, 11974133, 11674122, 11574112, 11474127, and

11634004), National Key Research and Development Program of China (grant no. 2016YFB0201204), Program for Changjiang Scholars and Innovative Research Team in University (grant no. IRT_15R23), and National Fund for Fostering Talents of Basic Science (grant no. J1103202). A.R.O. thanks Russian Science Foundation (grant no. 19-72-30043). D.V.S. thanks Russian Foundation for Basic Research, grant no. 19-03-00100 A. **Author contributions:** X.H., A.R.O., and T.C. conceived this project. D.Z., D.V.S., and X.H. performed the experiment. D.V.S., D.D. A.R.O., and T.C. prepared theoretical calculations and analysis. X.H., D.Z., D.V.S., A.R.O., and T.C. wrote and revised the paper. All authors discussed the results and offered the useful discussions. **Competing interests:** The authors declare that they have no competing interests. **Data and materials availability:** All data needed to evaluate the conclusions in the paper are present in the paper and/or the Supplementary Materials. Additional data related to this paper may be requested from the authors.

Submitted 13 April 2019
Accepted 25 November 2019
Published 28 February 2020
10.1126/sciadv.aax6849

Citation: D. Zhou, D. V. Semenok, D. Duan, H. Xie, W. Chen, X. Huang, X. Li, B. Liu, A. R. Oganov, T. Cui, Superconducting praseodymium superhydrides. *Sci. Adv.* **6**, eaax6849 (2020).

Science Advances

Superconducting praseodymium superhydrides

Di ZhouDmitrii V. SemenokDefang DuanHui XieWuhao ChenXiaoli HuangXin LiBingbing LiuArtem R. OganovTian Cui

Sci. Adv., 6 (9), eaax6849. • DOI: 10.1126/sciadv.aax6849

View the article online
https://www.science.org/doi/10.1126/sciadv.aax6849
Permissions
https://www.science.org/help/reprints-and-permissions

Science Advances (ISSN 2375-2548) is published by the American Association for the Advancement of Science. 1200 New York Avenue NW, Washington, DC 20005. The title *Science Advances* is a registered trademark of AAAS.